Journal of Statistical Physics, Vol. 101, Nos. 1/2, 2000

Non-Adiabatic Dynamics in Mixed Quantum-Classical Systems

Steve Nielsen,[1] Raymond Kapral,[1] and Giovanni Ciccotti[2]

Received December 16, 1999; final March 14, 2000

Non-adiabatic dynamics in mixed quantum-classical systems is investigated. The mixed quantum-classical system comprises a quantum system coupled to a classical environment. The starting point for the analysis is an evolution equation for the density matrix expressed in a basis of adiabatic quantum states that describes the full quantum dynamics of the subsystem and its coupling to the bath. Since the quantum dynamics influences the evolution of the "classical" degrees of freedom, a description in terms of single Newtonian trajectories is not possible. Through explicit calculations of a two-level quantum system coupled to a low dimensional bath we examine the details of mixed quantum-classical dynamics and its representation in terms of an ensemble of surface-hopping classical trajectory segments.

KEY WORDS: Surface-hopping dynamics; non-adiabatic dynamics; mixed quantum-classical dynamics; density matrix.

1. INTRODUCTION

The coupling between a quantum subsystem and an environment or bath can lead to complex dynamics in both the subsystem and bath. When the time scale on which the bath degrees of freedom change is long compared to that of the subsystem, one may make a Born–Oppenheimer approximation and solve the Schrödinger equation for the subsystem for fixed values of the bath coordinates. The resulting position-dependent adiabatic energies serve as the potential energies for the evolution of the bath. If the bath is assumed to be classical then its positions and momenta evolve

[1] Chemical Physics Theory Group, Department of Chemistry, University of Toronto, Toronto, Ontario M5S 3H6, Canada.
[2] INFM and Dipartimento di Fisica, Università "La Sapienza," Piazzale Aldo Moro, 2, 00185 Roma, Italy.

0022-4715/00/1000-0225$18.00/0

according to Newton's equations of motion in the Hellmann–Feynman forces derived from the adiabatic energies. This adiabatic description of the dynamics is applicable only if the motion of the bath is confined to a single adiabatic potential energy surface.

Such a simple description is not always appropriate. The coupling to a bath, either classical or quantum, may induce transitions among the adiabatic states. As a result it is no longer possible to describe the dynamics of the bath by a single phase space Newtonian trajectory.[1]

Starting from a Liouville equation for the density matrix of a mixed quantum-classical system that incorporates the full quantum dynamics of the subsystem and the "classical" dynamics of the bath, including their interactions, we investigate the nature of non-adiabatic dynamics. We show how the solution for the time evolution of the density matrix may be found in terms of an ensemble of surface-hopping trajectories. The trajectory description incorporates the coherent evolution of coupled quantum states induced by quantum transitions. We show how to concatenate the classical evolution segments to yield the time evolution and analyze the contributions to the density matrix arising from different numbers of quantum transitions.

Section 2 describes the evolution equation used in our study and expresses the density matrix in an adiabatic basis. The two-level model is introduced in Section 3 and the forms of the adiabatic and diabatic potential curves are described. A description of the dynamics in terms of approximate surface-hopping trajectories is presented in Section 4. In this section we study the phase space structure of the contributions to the density matrix arising from different numbers of quantum transitions. Finally, Section 5 contains the conclusions of this study.

2. EVOLUTION EQUATION

The quantum mechanical system we consider is partitioned into an n-particle subsystem and and an N-particle bath. Its Hamiltonian is

$$\hat{H} = \frac{\hat{P}^2}{2M} + \frac{\hat{p}^2}{2m} + \hat{V}(\hat{q}, \hat{Q}) \tag{1}$$

where $\hat{P}$ and M are the momentum operators and masses of the bath particles and $\hat{p}$ and m are the corresponding quantities for the subsystem particles. The total potential energy operator is $\hat{V}(\hat{q}, \hat{Q})$. We consider a representation in which we retain the Hilbert space description of the n-particle subsystem but carry out a Wigner transform[2] over the coordinates

of the N-particle bath.[3, 4] The partial Wigner transform of any operator $\hat{A}$ is defined by

$$\hat{A}_W(R, P) = \int dz\, e^{iP\cdot z/\hbar} \left\langle R - \frac{z}{2} \middle| \hat{A} \middle| R + \frac{z}{2} \right\rangle \tag{2}$$

Given this definition, the partially Wigner transformed Hamiltonian may be written as

$$\hat{H}_W(R, P) = \frac{P^2}{2M} + \frac{\hat{p}^2}{2m} + \hat{V}_W(\hat{q}, R) = \frac{P^2}{2M} + \hat{h}_W(R) \tag{3}$$

In this representation the bath state is characterized by the phase space coordinates (R, P) defined by the real parameters appearing in the Wigner transform. The second line of Eq. (3) defines the Hamiltonian $\hat{h}_W(R)$ whose eigenvalue problem is

$$\hat{h}_W(R)\,|\alpha; R\rangle = E_\alpha(R)\,|\alpha; R\rangle \tag{4}$$

Consequently, for every bath configuration R we may construct an adiabatic eigenfunction $|\alpha; R\rangle$ with corresponding eigenvalue $E_\alpha(R)$ and at each such configuration we have the completeness relation in the quantum subsystem space,

$$1 = \sum_\alpha |\alpha; R\rangle\langle \alpha; R| \tag{5}$$

In this adiabatic basis an element of the density matrix is given by $\rho_W^{\alpha\alpha'}(R, P) = \langle \alpha; R|\, \hat{\rho}_W(R, P)\, |\alpha'; R\rangle$. If we assume that the subsystem always remains in a single adiabatic state then the equation of motion for a diagonal element of the density matrix is simply determined by the evolution of the bath phase space coordinates in the Hellmann–Feynman forces for the particular quantum adiabatic state:

$$\begin{aligned} \frac{\partial \rho_W^\alpha(R, P, t)}{\partial t} &= -\{H_W^\alpha, \rho_W^\alpha(R, P, t)\} \\ &= -\left(\frac{P}{M}\cdot\frac{\partial}{\partial R} + F_W^\alpha \cdot \frac{\partial}{\partial P}\right)\rho_W^\alpha(R, P, t) \end{aligned} \tag{6}$$

where $\{\cdot, \cdot\}$ denotes the Poisson bracket and $\rho_W^\alpha(R, P, t) \equiv \rho_W^{\alpha\alpha}(R, P, t)$. Here $F_W^\alpha = -\langle \alpha; R|\, \partial \hat{V}_W(\hat{q}, R)/\partial R\, |\alpha; R\rangle = -\partial E_\alpha/\partial R$ is the Hellmann–Feynman force for state α.

Let $iL_\alpha = (P/M)\cdot\nabla_R + F^\alpha_W\cdot\nabla_P$ be the classical Liouville operator for evolution under the Hellmann–Feynman force F^α_W. Given the phase space point (R, P) at time t its backward evolution to time $t=0$ is denoted by

$$(R_{\alpha,0}, P_{\alpha,0}) = e^{-iL_\alpha t}(R, P) \tag{7}$$

Thus the solution of Eq. (6) is

$$\rho^\alpha_W(R, P, t) = e^{-iL_\alpha t}\rho^\alpha_0(R, P) = \rho^\alpha_0(R_{\alpha,0}, P_{\alpha,0}) \tag{8}$$

where $\rho^\alpha_0(R, P)$ is the initial value of the density matrix. Consequently, the solution of the adiabatic dynamics simply involves the solution of the classical equations of motion, and the bath phase space point follows a single Newtonian trajectory.

This is no longer the case when transitions among the quantum adiabatic states may occur. To compute the non-adiabatic dynamics of a quantum subsystem coupled to a classical bath we must generalize Eq. (6). Suppose the entire system is described quantum mechanically and the density matrix evolves according to the quantum Liouville equation,

$$\frac{\partial\hat\rho}{\partial t} = -\frac{i}{h}[\hat H, \hat\rho] \tag{9}$$

The mixed quantum-classical Liouville equation is obtained by taking the partial Wigner transform of this equation and evaluating the Liouville operator to lowest order in the mass ratio $\mu = (m/M)^{1/2}$ to yield,

$$\frac{\partial\hat\rho_W(R, P, t)}{\partial t} = -\frac{i}{h}[\hat H_W, \hat\rho_W] + \frac{1}{2}(\{\hat H_W, \hat\rho_W\} - \{\hat\rho_W, \hat H_W\}) \tag{10}$$

Expressing this equation in the adiabatic basis we find[3]

$$\frac{\partial\rho^{s_i}_W(R, P, t)}{\partial t} = \sum_{s_j} -i\mathscr{L}_{s_i s_j}\rho^{s_j}_W(R, P, t) \tag{11}$$

where

$$-i\mathscr{L}_{s_i, s_j} = (-i\omega_{s_i} - iL_{s_i})\,\delta_{r^0_{ij}}\delta_{r^1_{ij}} + J_{s_i s_j} \tag{12}$$

In writing this equation we have used the notation $s_i = \alpha_i\alpha'_i$, $r^0_{ij} = \alpha_i\alpha_j$ and $r^1_{ij} = \alpha'_i\alpha'_j$. The subscripts i and j denote different values of α and α' that

occur in the course of the dynamics. The adiabatic frequency difference is defined by $\omega_{s_i}(R) = (E_{\alpha_i}(R) - E_{\alpha_i'}(R))/\hbar$, while the Liouville operator iL_{s_i} involves the mean of the Hellmann–Feynman forces of the two quantum states labeling the density matrix element and is given by the expression,

$$iL_{s_i} = \frac{P}{M} \cdot \frac{\partial}{\partial R} + \frac{1}{2}(F_W^{\alpha_i} + F_W^{\alpha_i'}) \cdot \frac{\partial}{\partial P} \tag{13}$$

The second term in Eq. (12) is responsible for coupling the different adiabatic states and is given by

$$J_{s_i s_j} = -\sum_{\kappa=0}^{1} \left\{ \frac{P}{M} \cdot d_{ij}^{\kappa} + \frac{1}{2} \Delta E_{ij}^{\kappa} d_{ij}^{\kappa} \cdot \frac{\partial}{\partial P} \right\} \delta_{r_{ij}^{1-\kappa}} \tag{14}$$

with the non-adiabatic coupling matrix defined as $d_{ij}^0 = \langle \alpha_i; R | \partial/\partial R | \alpha_j; R \rangle$, $d_{ij}^1 = \langle \alpha_i'; R | \partial/\partial R | \alpha_j'; R \rangle^*$, $\Delta E_{ij}^0 = E_{\alpha_i} - E_{\alpha_j}$ and $\Delta E_{ij}^1 = E_{\alpha_i'} - E_{\alpha_j'}$. We see that if the coupling term $J_{s_i s_j}$ is set to zero, the diagonal elements of the density matrix evolve according to adiabatic dynamics as in Eq. (6). Due to the presence of J a description in terms of a single Newtonian trajectory is no longer possible. However, the solution may be represented by an ensemble of surface-hopping trajectories where classical evolution segments are interrupted by quantum transitions.

3. TWO-LEVEL SYSTEM

To illustrate some of the features of non-adiabatic mixed quantum-classical dynamics we consider a two-level system coupled to a classical bath[5] whose Hamiltonian matrix, expressed in the diabatic basis $\{|1d\rangle, |2d\rangle\} = \{(|1\rangle + |2\rangle)/\sqrt{2}, (|1\rangle - |2\rangle)/\sqrt{2}\}$, where $|1\rangle$ and $|2\rangle$ are the quantum subsystem eigenstates, may be written as[6]

$$\mathbf{h}_W(R) = -\tfrac{1}{2}\hbar\Delta\sigma_x + \varepsilon(R)\,\mathbf{I} + \hbar\gamma(R)\,\sigma_z \tag{15}$$

Here $\varepsilon(R) = \bar{\varepsilon} + V_b(R)$, with $\bar{\varepsilon}$ the mean energy of the two subsystem states and $V_b(R)$ the bath potential energy, Δ is the energy gap in $\hbar$ units, $\gamma(R)$ determines the coupling to the bath, $\mathbf{I}$ is the unit matrix and $\boldsymbol{\sigma}$ is the Pauli spin matrix. The adiabatic eigenvalues and eigenfunctions of $\mathbf{h}_W$ are

$$E_{1,2}(R) = \varepsilon(R) \pm \frac{\hbar}{2}(\Delta^2 + 4\gamma(R)^2)^{1/2} \tag{16}$$

and

$$\begin{aligned} |1; R\rangle &= (2(1+G^2))^{-1/2}\,((1+G)\,|1d\rangle + (1-G)\,|2d\rangle) \\ |2; R\rangle &= (2(1+G^2))^{-1/2}\,((1-G)\,|1d\rangle - (1+G)\,|2d\rangle) \end{aligned} \tag{17}$$

with

$$G(R) = (2\gamma(R))^{-1}\,(-\Delta + (\Delta^2 + 4\gamma(R)^2)^{1/2}) \tag{18}$$

As an example suppose the bath is one dimensional with a bistable potential of the form,

$$V_b(R) = \frac{a}{4}R^4 - \frac{b}{2}R^2 \tag{19}$$

and the coupling to the two-level system is $\gamma(R) = \gamma_0(R + c_2R^2)$. When presenting numerical results we use dimensionless variables obtained by making the replacements $\bar{t} = t\omega_0$, $\bar{R} = (h/(M\omega_0))^{-1/2}\,R$, $\bar{P} = (hM\omega_0)^{-1/2}\,P$, where ω_0 is a characteristic frequency, with similar dimensionless forms for the potential and coupling parameters that follow from these variable changes. For what follows we drop the overbars on dimensionless variables to simplify the notation.

The adiabatic energies as a function of R are sketched in Figs. 1 and 2 for $c_2 = 0.0$ and $c_2 = 1.0$ with the other parameters fixed as indicated in the caption.

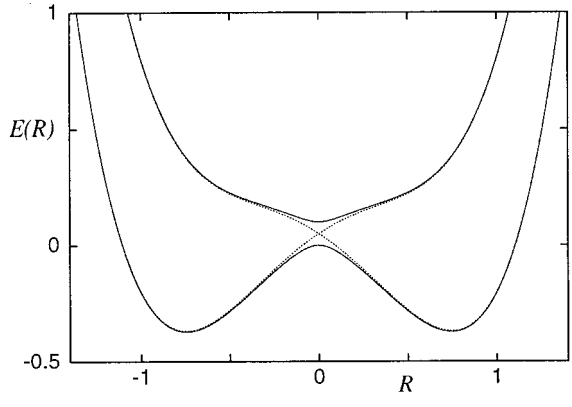

Fig. 1. Adiabatic (solid lines) and diabatic (dashed lines) energies versus R for the parameters: $a = 3.0$, $b = 1.0$, $\Delta = 0.1$, $\gamma_0 = 0.5$ and $c_2 = 0.0$.

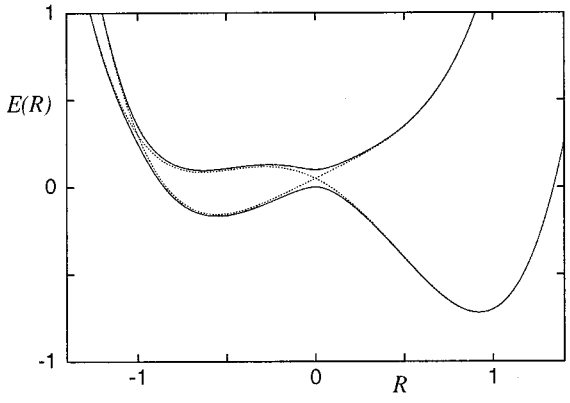

Fig. 2. Adiabatic and diabatic energies versus R. Labeling and parameters same as in Fig. 1 except $c_2 = 1.0$.

The diabatic energies (dashed lines in Figs. 1 and 2) are given by the diagonal elements of $\mathbf{h}_W(R)$, $E^d_{1,2}(R) = \varepsilon(R) \pm \hbar\gamma(R)$. Note that there is a single crossing of the diabatic curves when $c_2 = 0.0$ (Fig. 1) and two such crossings when $c_2 = 1.0$ (Fig. 2). Thus, we may expect rather different non-adiabatic dynamics in these two cases.

4. APPROXIMATE SURFACE HOPPING TRAJECTORIES

The mixed quantum-classical Liouville equation (11) may be integrated and the resulting integral equation solved by iteration to yield an expression for $\rho^{s_0}_W(R, P, t)$ in terms of its initial value $\rho^{s_i}_0(R, P)$:[3]

$$\begin{aligned}\rho^{s_0}_W(R, P, t) = {} & e^{-(i\omega_{s_0} + iL_{s_0})\, t}\rho^{s_0}_0(R, P) + \sum_{s_1}\int_0^t d\tau_1 \\ & \times e^{-(i\omega_{s_0} + iL_{s_0})(t-\tau_1)} J_{s_0 s_1} e^{-(i\omega_{s_1} + iL_{s_1})\,\tau_1}\rho^{s_1}_0(R, P) \\ & + \sum_{s_1}\sum_{s_2}\int_0^t d\tau_1 \int_0^{\tau_1} d\tau_2\, e^{-(i\omega_{s_0} + iL_{s_0})(t-\tau_1)} \\ & \times J_{s_0 s_1} e^{-(i\omega_{s_1} + iL_{s_1})(\tau_1 - \tau_2)} J_{s_1 s_2} e^{-(i\omega_{s_2} + iL_{s_2})\,\tau_2}\rho^{s_2}_0(R, P) + \cdots \end{aligned} \quad (20)$$

This expression for the density matrix may be evaluated exactly using a hybrid Molecular Dynamics–Monte Carlo scheme. The exact simulation method involves following a branching tree of trajectories since each time a momentum derivative in J acts two new trajectories are spawned when

the derivative is evaluated using finite differences.[7] It is possible to construct a simpler trajectory picture if the J operator is evaluated in the momentum jump approximation,[3]

$$\begin{aligned} J_{s_i s_j} &= -\sum_{\kappa=0}^{1} \frac{P}{M} \cdot d_{ij}^{\kappa} \left\{ 1 + \frac{1}{2} S_{ij}^{\kappa} \cdot \frac{\partial}{\partial P} \right\} \delta_{r_{ij}^{1-\kappa}} \\ &\approx -\sum_{\kappa=0}^{1} \frac{P}{M} \cdot d_{ij}^{\kappa} e^{1/2\, S_{ij}^{\kappa} \cdot \nabla_P} \delta_{r_{ij}^{1-\kappa}} \end{aligned} \tag{21}$$

where $S_{ij}^{\kappa} = \Delta E_{ij}^{\kappa} d_{ij}^{\kappa} ((P/M) \cdot d_{ij}^{\kappa})^{-1}$. The effect of the action of J on any function of P is to increment P by $S_{ij}^{\kappa}/2$, $P \to P + S_{ij}^{\kappa}/2$, since J is now a momentum translation operator.

Using this form for J and backward-evolved trajectory segments defined as

$$\begin{aligned} (R_{s_0,\tau_1}, P_{s_0,\tau_1}) &= e^{-iL_{s_0}(t-\tau_1)}(R, P) \\ (R_{s_2,\tau_2}^{\tau_1,\kappa_1}, P_{s_1,\tau_2}^{\tau_1,\kappa_1}) &= e^{-iL_{s_1}(\tau_1-\tau_2)} \left(R_{s_0,\tau_1}, P_{s_0,\tau_1} + \frac{S_1^{\kappa_1}}{2} \right) \\ &\cdots \\ (R_{s_i,\tau_{i+1}}^{\{\tau_i,\kappa_i\}}, P_{s_i,\tau_{i+1}}^{\{\tau_i,\kappa_i\}}) &= e^{-iL_{s_i}(\tau_i-\tau_{i+1})} \left(R_{s_{i-1},\tau_i}^{\{\tau_{i-1},\kappa_{i-1}\}}, P_{s_{i-1},\tau_i}^{\{\tau_{i-1},\kappa_{i-1}\}} + \frac{S_i^{\kappa_i}}{2} \right) \end{aligned} \tag{22}$$

we may write the series solution of the density matrix in a form that may be evaluated directly using the hybrid MD–MC procedure. We have[3,7]

$$\begin{aligned} &\rho_W^{s_0}(R, P, t) \\ &= \mathscr{W}_{s_0}(t, 0)\, \rho_0^{s_0}(R_{s_0,0}, P_{s_0,0}) - \sum_{s_1} \sum_{\kappa_1} \int_0^t d\tau_1\, \mathscr{W}_{s_0}(t, \tau_1) \\ &\quad \times \frac{P_{s_0,\tau_1}}{M} \cdot d_1^{\kappa_1}(R_{s_0,\tau_1})\, \mathscr{W}_{s_1}(\tau_1, 0)\, \rho_0^{s_1}(R_{s_1,0}^{\{\tau_1,\kappa_1\}}, P_{s_1,0}^{\{\tau_1,\kappa_1\}}) \\ &\quad + \sum_{s_1, s_2} \sum_{\kappa_1, \kappa_2} \int_0^t d\tau_1 \int_0^{\tau_1} d\tau_2\, \mathscr{W}_{s_0}(t, \tau_1) \frac{P_{s_0,\tau_1}}{M} \cdot d_1^{\kappa_1}(R_{s_0,\tau_1})\, \mathscr{W}_{s_1}(\tau_1, \tau_2) \\ &\quad \times \frac{P_{s_1,\tau_2}^{\{\tau_1,\kappa_1\}}}{M} \cdot d_2^{\kappa_2}(R_{s_1,\tau_2}^{\{\tau_1,\kappa_1\}})\, \mathscr{W}_{s_2}(\tau_2, 0)\, \rho_0^{s_2}(R_{s_2,0}^{\{\tau_2,\kappa_2\}}, P_{s_2,0}^{\{\tau_2,\kappa_2\}}) + \cdots \end{aligned} \tag{23}$$

Here $d_i^{\kappa} \equiv d_{i-1,i}^{\kappa}$, $\{\tau_i, \kappa_i\} = ((\tau_1, \kappa_1), (\tau_2, \kappa_2), ..., (\tau_i, \kappa_i))$ and the $\mathscr{W}$ phase factors are given by

$$\mathscr{W}_{s_i}(\tau_i, \tau_{i+1}) = e^{i \int_{\tau_i}^{\tau_{i+1}} d\tau\, \omega_{s_i}(R_{s_i,\tau}^{\{\tau_i, \kappa_i\}})} \tag{24}$$

For the one-dimensional bath considered here, the Hellmann–Feynman force appearing in the classical evolution operator is

$$F_W^{1,2} = F_b(R) \mp 2h\gamma(R)\, \gamma'(R)(\Delta^2 + 4\gamma(R)^2)^{-1/2} \tag{25}$$

while the quantity that determines the momentum change $S_{12}^0 = -S_{21}^0$ appearing in J is given by

$$S_{12}^0 = ((\Delta^2 + 4\gamma(R)^2)^{1/2} \left(\frac{P}{M}\right)^{-1} \tag{26}$$

and is plotted in Fig. 3 for $c_2 = 0.0$.

The non-adiabatic coupling matrix element is

$$d_{12}^0 = -d_{21}^0 = d_{12}^1 = \frac{G'}{(1+G^2)} \tag{27}$$

and is sketched in Fig. 4.

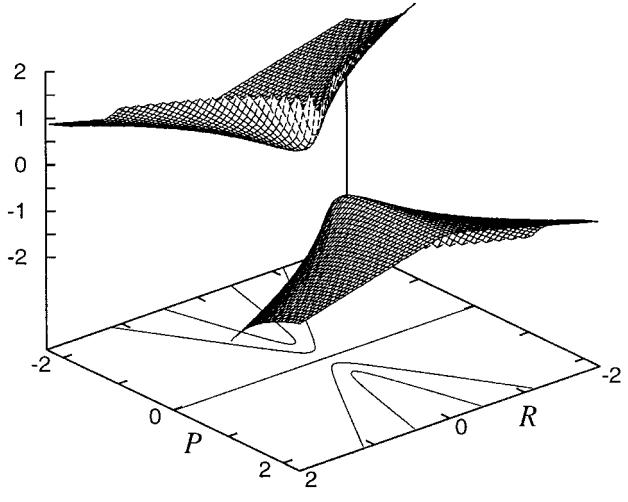

Fig. 3. Phase space plot of S_{12} for the parameters in Fig. 1.

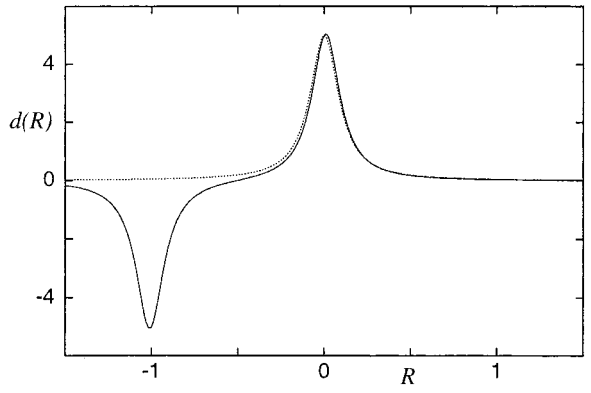

Fig. 4. Non-adiabatic coupling matrix elements for the parameters in Figs. 1 and 2; dotted line ($c_2 = 0.0$), solid line ($c_2 = 1.0$).

The non-adiabatic coupling matrix element has a single maximum in the vicinity of the single diabatic curve crossing for $c_2 = 0.0$ but has two extrema for $c_2 = 1.0$.

In order to compute the terms in the series for the time evolution of the density matrix we use a Monte Carlo method to evaluate the integrals and sums in conjunction with molecular dynamics. For a term with n quantum transitions, we sample the quantum state and the time at which the transitions occur from suitable distributions. In particular, if there are ℓ quantum states, for a transition $\alpha_i \to \alpha_{i+1}$ or $\alpha'_i \to \alpha'_{i+1}$ the final value of α or α' is chosen with probability $p(\alpha) = (\ell - 1)^{-1}$. The times at which the transitions occur are chosen from uniform distributions such that $p(\tau_i) = \tau_{i-1}^{-1}$. The two terms in J are labeled by $\kappa = 0$ or $\kappa = 1$. Which term acts is determined by a Bernoulli trial in the following way: the term with $\kappa_i = 0$ is chosen with probability $p(\kappa_i = 0) = \varphi_i$ while the term with $\kappa_i = 1$ is chosen with probability $p(\kappa_i = 1) = 1 - \varphi_i$ where

$$\varphi_i = \frac{1}{\Upsilon_i} \frac{Q_i^{\kappa_i}}{1 + Q_i^{\kappa_i}} \tag{28}$$

with

$$\Upsilon_i = \sum_{\kappa_i} \frac{Q_i^{\kappa_i}}{1 + Q_i^{\kappa_i}} \tag{29}$$

In these equations,

$$Q_i^{\kappa_i} = \left| \frac{P_{s_{i-1}, \tau_i}^{\{\tau_{i-1}, \kappa_{i-1}\}}}{M} \cdot d_i^{\kappa_i}(R_{s_{i-1}, \tau_i}^{\{\tau_{i-1}, \kappa_{i-1}\}}) \right| \tag{30}$$

For a two-level system these general results take a simple form: the choice of quantum state not currently occupied is determined with probability one and the terms in J are chosen with probability 1/2.

4.1. Simulation Results

We begin with a discussion of the results for $c_2 = 0.0$ where there is a single crossing of the diabatic curves as shown in Fig. 1. We consider an initial condition where only the excited adiabatic state (labeled 2) is populated,

$$\rho_0^{22}(R, P) = \frac{1}{2\pi\sigma_R\sigma_P} \exp(-R^2/2\sigma_R^2) \exp(-P^2/2\sigma_P^2) \tag{31}$$

with $\sigma_R = \sigma_P = 1$ and focus on the phase space structure of $\rho_W^{22}(R, P, t)$. It is clear from the form of Eq. (20) that we get a non-zero contribution to $\rho_W^{22}(R, P, t)$ only for terms with an even number of quantum transitions where the trajectories return to the excited state potential curve. Figure 5

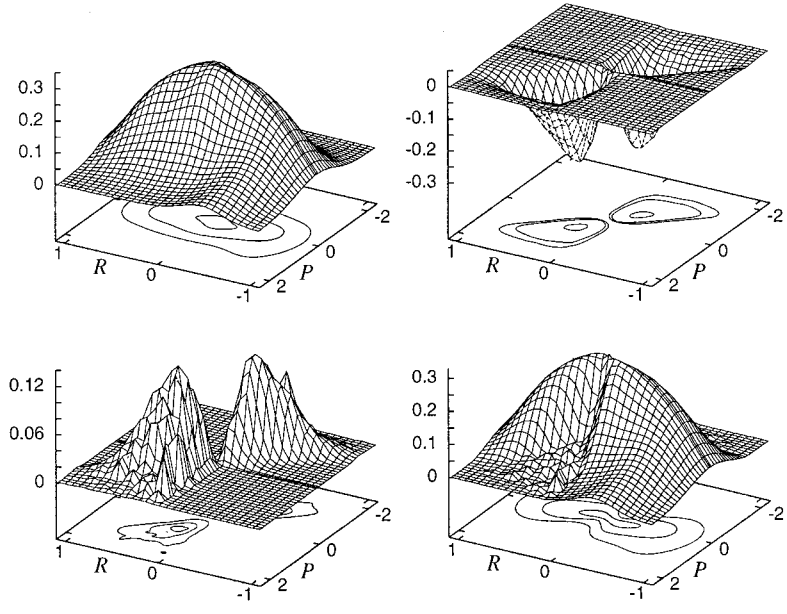

Fig. 5. Zeroth (upper left), second (upper right) and fourth (lower left) order contributions to $\rho_W^{22}(R, P, t = 0.6)$ for $c_2 = 0.0$. The sum of these three contributions is displayed in the lower right panel.

plots the zeroth (adiabatic dynamics), second and fourth order contributions along with their sum which provides an approximation to this density matrix element.

The form of the adiabatic contribution simply reflects the nature of the classical dynamics on the excited state adiabatic curve which has a minimum at $R=0$. Since the potential energy is not parabolic the distribution distorts as time evolves.

The second and fourth order terms exhibit pronounced bimodal structure. In order to analyse the form of the second order term it is useful to examine the trajectories which enter in its computation. The second order term is the third term on the right hand side of Eq. (23). One can see that the phase space points required are $(R_{22,\tau_1}, P_{22,\tau_1})$, $(R_{12,\tau_2}^{\{\tau_1,\kappa_1\}}, P_{12,\tau_2}^{\{\tau_1,\kappa_1\}})$ and $(R_{22,0}^{\{\tau_2,\kappa_2\}}, P_{22,0}^{\{\tau_2,\kappa_2\}})$. Starting from an ensemble of phase space points (R, P) at time t drawn from a uniform distribution over a finite domain large enough to encompass all but the vanishingly small tails of the distributions of interest, we examine the phase space distribution of the ensemble.

The first quantum transition occurs at times $\tau_1 \in (0, t)$ and Fig. 6 (upper left panel) shows a contour plot of the histogram of the phase space points $(R_{22,\tau_1}, P_{22,\tau_1})$ for all $\tau_1 - \varepsilon$ just prior to the transition while the upper right panel shows this quantity for all $\tau_1 + \varepsilon$ just after the transition. For each surface hopping trajectory which contributes to the histograms shown in Fig. 6, τ_1 and τ_2 are sampled uniformly from $(0, t)$ and $(0, \tau_1)$ respectively.

One sees the depletion of trajectory phase space points which may be ascribed solely to the momentum jump. Since the transition must take place from the excited state to the ground state, $2 \to 1$, the momentum jump factor $S_{21} = (E_2 - E_1)/(P/M)$ will always increase the magnitude of the momentum of the classical bath since $E_2 - E_1 > 0$ and consequently S_{21} has the same sign as P. Given the form of S_{12} ($S_{12} = -S_{21}$) in Fig. 3, this accounts for the depletion zone that arises in the passage from the upper left to upper right panels of the figure.

Similarly, the next transition that appears in the second order term involves a transition from the ground state to the excited state, $1 \to 2$, and S_{12} has a sign opposite to that of P causing trajectories to slow down or reverse directions. The contour plots of the histograms of trajectories just prior to, $\tau_2 - \varepsilon$, and just after, $\tau_2 + \varepsilon$, the second quantum transition are shown in lower panels of Fig. 6. Note that although the d_{12} non-adiabatic coupling matrix element is determined by the two adiabatic states, the dynamics occurs on the potential curve determined by the mean of the two adiabatic states since they are coherently coupled as a result of the first quantum transition. For the two-level model this mean potential is just the bare classical bath potential plus a constant, $(E_1(R) + E_2(R))/2 = \bar{\varepsilon} + V_b(R)$.

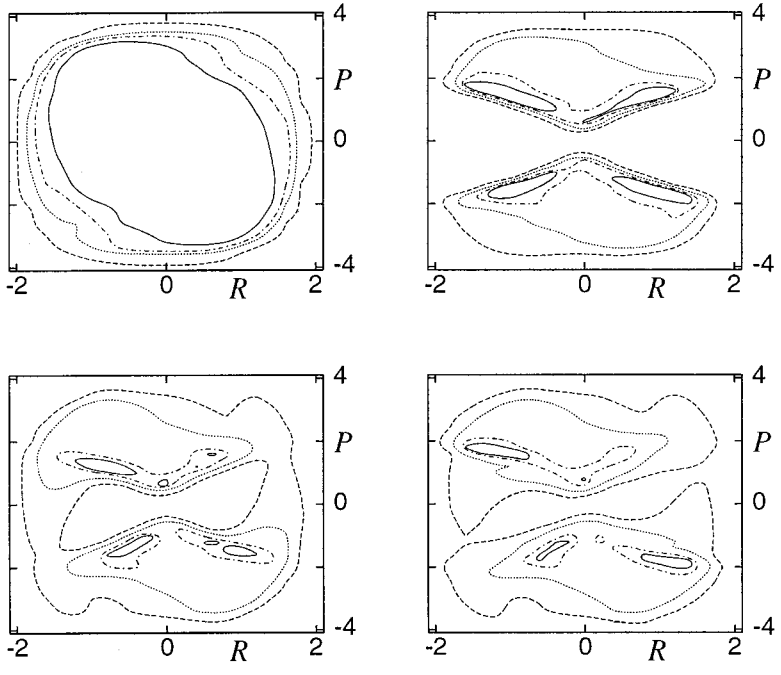

Fig. 6. Contour plots of the normalized histograms of phase space points just prior to and just after quantum transitions contributing to the second order term in the density matrix element $\rho_W^{22}(R, P, t = 0.6)$. Upper left panel: contours at 0.04 (solid line), 0.02 (dash-dot), 0.01 (dot), 0.001 (dash). Remaining three panels: contours at 0.10 (solid line), 0.075 (dash-dot), 0.04 (dot), 0.01 (dash). See text for details.

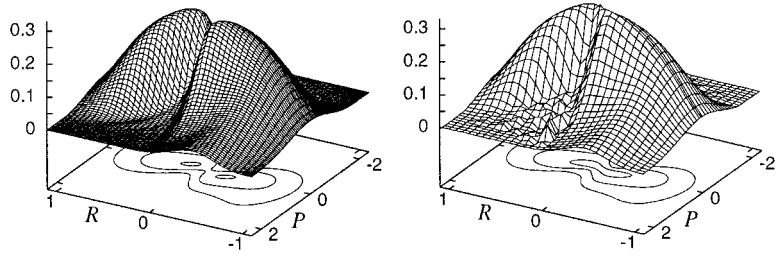

Fig. 7. The exact form of $\rho_W^{22}(R, P, t = 0.6)$ obtained by solving the coupled partial differential equations for the density matrix elements by finite differences is shown in the left hand panel. The right hand panel shows the corresponding momentum jump approximation (also shown in the lower right hand panel of Fig. 5).

The phase space form of the density matrix element in Fig. 5 (lower right panel) was checked by solving the coupled partial differential equations for the density matrix elements by finite differences [see Eq. (11)]. This result is shown in Fig. 7. The two forms of ρ_W^{22} are nearly identical with the exception of a small region around the origin $(R, P) = (0, 0)$. The behavior at the origin bears special mention. The origin is either a stable or an unstable fixed point under the adiabatic dynamics (upper and lower solid curves of Fig. 1 respectively). Consequently, in the momentum jump treatment trajectories which are propagated backwards from the origin experience an infinitely large momentum jump. Viewed as a limiting process, as P appoaches zero the momentum jump S_{12} becomes arbitrarily large [see Eq. (26)]. This has the effect of ejecting such trajectories to the tails of the initial distribution ρ_0^{22}, giving them a vanishing weight in all terms of Eq. (23) which involve one or more quantum transitions. This is manifested in the upper right and lower left panels of Fig. 5 as a complete separation of the two lobes, and also in the right hand panel of Fig. 7 as a unimodal profile along the curve $P = 0$. The correct behavior around the origin is bimodal.

For the momentum jump approximation to be plausible we require (without any *a priori* knowledge of the contribution from the gradient term) S to be small [see Eq. (21) and Eq. (26)], but S is manifestly large for small momentum values. Thus from the nature of the approximation we expect problems when P is small. This discrepancy is revealed in Fig. 8, which shows the population f_2 and the average values of R^2 and P^2,

$$f_i = \int dR\, dP\, \rho_W^{ii} \tag{32}$$

$$\langle R^2 \rangle_i = \int dR\, dP\, R^2 \rho_W^{ii} \tag{33}$$

$$\langle P^2 \rangle_i = \int dR\, dP\, P^2 \rho_W^{ii} \tag{34}$$

versus time for the density matrix element ρ_W^{22} in both the momentum jump approximation (up to sixth order) and the finite difference solution. The population (the populations in the excited and ground states are related by $f_1 + f_2 = 1$) and $\langle R^2 \rangle_2$ values are in excellent agreement between these two solutions. The deviation of the $\langle P^2 \rangle_2$ momentum jump curve from its exact value reflects the approximate treatment of momentum changes in the bath. Figure 9 decomposes the $\langle R^2 \rangle_2$ curve of Fig. 8 into its constituent parts in order to illustrate the convergence of the series of Eq. (23). Two general features emerge from an examination of Fig. 9 and of the

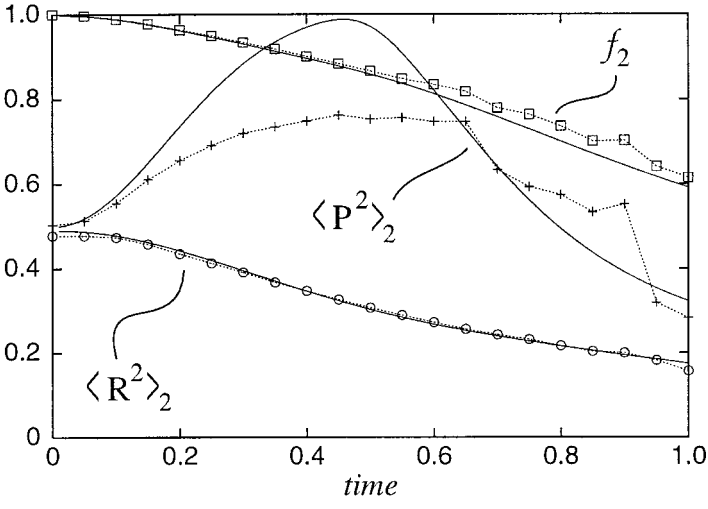

Fig. 8. The population f_2 and the average values $\langle R^2 \rangle_2$ and $\langle P^2 \rangle_2$ versus time are shown for the density matrix element ρ_W^{22} in both the momentum jump approximation (up to sixth order, shown with symbols) and the finite difference solution (shown in the solid line).

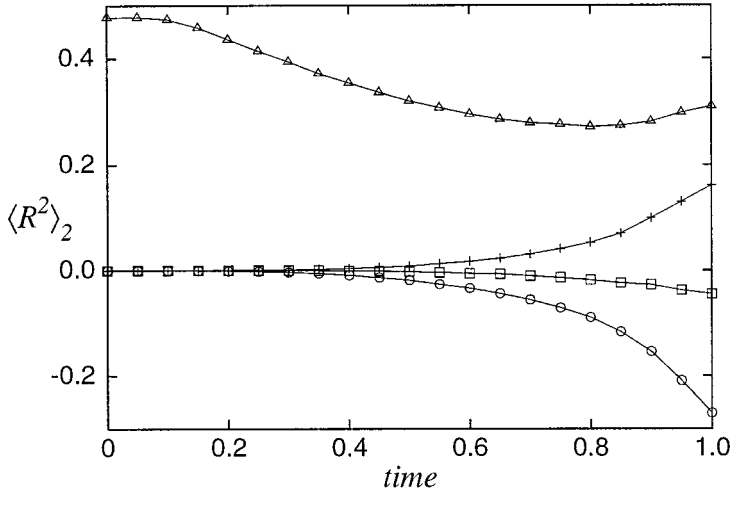

Fig. 9. The $\langle R^2 \rangle_2$ curve of Fig. 8 is decomposed into its constituent parts; namely the first term on the right hand side of Eq. (23) with $s_0 = 22$ (shown with $\triangle$), the third term (shown with $\bigcirc$), the fifth term (shown with $+$), and the seventh term (shown with $\square$). The second, fourth, sixth, etc. terms on the right hand side of Eq. (23) are identically zero for the case of $s_0 = 22$ and with the initial conditions given by Eq. (31).

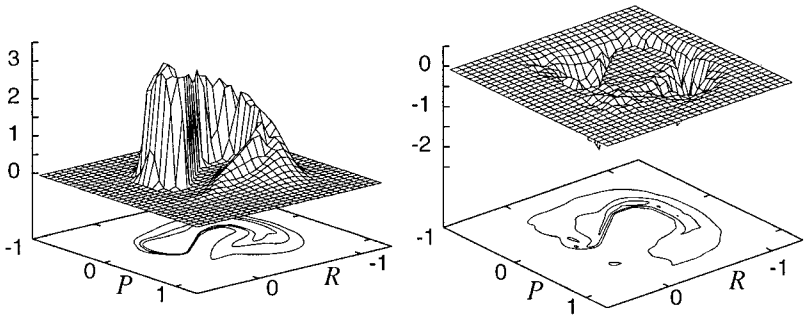

Fig. 10. Zeroth (left panel) and second (right panel) order contributions to $\rho_W^{22}(R, P, t = 3.33)$ for $c_2 = 1.0$.

corresponding decompositions for the population and $\langle P^2 \rangle_2$ curves (not shown); namely that each subsequent term in the series of Eq. (23) tends to be smaller in absolute value than its predecessor, and that more and more terms are needed to obtain a good estimate of the full series solution as time increases.

When $c_2 = 1.0$ one has more complex non-adiabatic dynamics due to the existence of two diabatic curve crossings and additional structure in the adiabatic energy curves. The initial condition was again taken to be a Gaussian on the excited adiabatic curve but its width is narrower, $\sigma_R = \sigma_P = 1/2\sqrt{5}$, than that for the $c_2 = 0.0$ case in order to have the initial density lie largely in the vicinity of the potential minimum near $R = 0$. Figure 10 presents information for $c_2 = 1.0$ similar to that in Fig. 5 (upper panels) but at a longer time $t = 3.33$.

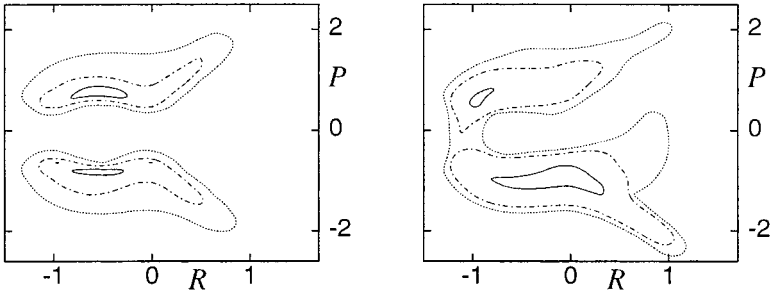

Fig. 11. Contour plots of the normalized histograms of phase space points just after quantum transitions contributing to the second order term in the density matrix element $\rho_W^{22}(R, P, t = 3.33)$. Left panel, after the first transition; contours at 0.40 (solid line), 0.25 (dash-dot), 0.05 (dot). Right panel, after the second transition; contours at 0.25 (solid line), 0.10 (dash-dot), 0.05 (dot). See text for additional details.

If one analyses the phase space points that enter in the factors of the second order term as a result of the momentum jumps that accompany the quantum transitions, one see the richer structure shown in Fig. 11. This figure presents contour plots of the histograms of the phase space points just after the first and second quantum transitions at times $\tau_1 + \varepsilon$, $\tau_1 \in (0, t)$ and $\tau_2 + \varepsilon$, $\tau_2 \in (0, \tau_1)$.

As in the earlier discussion, the left panel of this figure directly reflects the form of S_{12}, which is more complex because the energy difference $\Delta E_{12}(R)$ has additional features because both the excited and ground adiabatic curves have two minima. The form of the phase space histogram after the second transition is determined by the evolution on the bath potential curve and the momentum jump associated with the transition back to the excited state.

5. CONCLUSIONS

It is often a good approximation to treat a subset of the degrees of freedom of a system classically while retaining the quantum character of the remaining degrees of freedom.[8] This is true for spin systems, electrons or protons embedded in a bath composed of heavy molecules, etc. There has been considerable effort devoted to the formulation of methods for treating mixed quantum-classical dynamics, including schemes based on mean field approximations,[9] solutions of the density matrix equation that treat the bath phenomenologically[10] and dynamics based on surface-hopping descriptions of the dynamics.[11–13]

The mixed quantum-classical Liouville equation that forms the starting point for the computations presented here reduces to the quantum Liouville equation for the subsystem and the classical Liouville equation for the bath when coupling between the the two systems is neglected. The coupling term is responsible both for quantum transitions and momentum changes in the bath that accompany these transitions. The calculations presented in the paper demonstrate how the density matrix evolves in the presence of coupling and how mean values of the quantum subsystem and bath variables vary with time and are influenced by quantum transitions. The approximate surface-hopping description in Section 4 shows how to construct an ensemble of trajectories that yields the solution of the density matrix. The structure of the results indicate how quantum transitions induce coherent evolution of pairs of quantum states and what trajectories contribute to a particular pair of quantum states at a particular classical phase space point of the bath. Examination of the contributions to the density matrix arising from different numbers of quantum transitions show how adiabatic dynamics is modified in the presence of quantum transitions.

While we have not discussed the surface-hopping method in detail here, we note that it is possible to construct hybrid MD-MC schemes that allow one to simulate the exact solution of the mixed quantum-classical Liouville equation without recourse to the momentum-jump approximation.[7] However, in many instances the momentum-jump approximation is appropriate and provides a simpler picture of the evolution of the ensemble of trajectories. The exact solution requires that one follow an ensemble of branching trajectories in order to compute the momentum derivatives in J. Both of these schemes allow one to treat classical baths with large numbers of degrees of freedom with arbitrarily complex potentials. Hence, the surface-hopping method described here can be applied to physically relevant many-body problems.

ACKNOWLEDGMENTS

This work was supported in part by a grant from the Natural Sciences and Engineering Research Council of Canada.

REFERENCES

1. P. Pechukas, *Phys. Rev.* **181**:166, 174 (1969).
2. E. Wigner, *Phys. Rev.* **40**:749 (1932); K. Imre, E. Özizmir, M. Rosenbaum, and P. F. Zwiefel, *J. Math. Phys.* **5**:1097 (1967).
3. R. Kapral and G. Ciccotti, *J. Chem. Phys.* **110**:8919 (1999).
4. W. Y. Zhang and R. Balescu, *J. Plasma Phys.* **40**:199 (1988); R. Balescu and W. Y. Zhang, *J. Plasma Phys.* **40**:215 (1988).
5. Two-level mixed quantum-classical systems have been considered in C. C. Martens and J.-Y. Fang, *J. Chem. Phys.* **106**:4918 (1996); A. Donoso and C. C. Martens, *J. Phys. Chem.* **102**:4291 (1998).
6. See, for example, A. J. Leggett, S. Chakravarty, A. T. Dorsey, M. P. A. Fisher, A. Garg, and W. Zwerger, *Rev. Mod. Phys.* **59**:1 (1987).
7. S. Nielsen, R. Kapral, and G. Ciccotti, *J. Chem. Phys.* **112**, April 15 (2000).
8. J. C. Tully, in *Modern Methods for Multidimensional Dynamics Computations in Chemistry*, D. L. Thompson, ed. (World Scientific, New York, 1998), p. 34; M. F. Herman, *Annu. Rev. Phys. Chem.* **45**:83 (1994).
9. H. J. Berendsen and J. Mavri, *J. Phys. Chem.* **97**:13464 (1993); P. Bala, B. Lesyng, and J. A. McCammon, *Chem. Phys. Lett.* **219**:259 (1994); F. A. Bornemann, P. Nettesheim, and C. Schütte, *J. Chem. Phys.* **105**:1074 (1996).
10. Y. Tanimura and S. Mukamel, *J. Chem. Phys.* **101**:3094 (1994).
11. J. C. Tully, *J. Chem. Phys.* **93**:1061 (1990); J. C. Tully, *Int. J. Quantum Chem.* **25**:299 (1991); D. S. Sholl and J. C. Tully, *J. Chem. Phys.* **109**:7702 (1998); S. Hammes-Schiffer and J. C. Tully, *J. Chem. Phys.* **101**:4657 (1994); Kohen, F. Stillinger, and J. C. Tully, *J. Chem. Phys.* **109**:4713 (1998).
12. L. Xiao and D. F. Coker, *J. Chem. Phys.* **100**:8646 (1994); D. F. Coker and L. Xiao, *J. Chem. Phys.* **102**:496 (1995); H. S. Mei and D.F. Coker, *J. Chem. Phys.* **104**:4755 (1996).
13. F. Webster, P. J. Rossky, and P. A. Friesner, *Comp. Phys. Comm.* **63**:494 (1991); F. Webster, E. T. Wang, P. J. Rossky, and P. A. Friesner, *J. Chem. Phys.* **100**:483 (1994).